Paper 38.6

A MONO-MODAL FIBER-OPTICS VELOCIMETER FOR ELECTROCHEMICALLY-GENERATED BUBBLES

R. Wedin[1,2,*], L. Davoust[1,**], A. Cartellier[1] and A. Dahlkild[2]
[1]LEGI, Domaine universitaire, BP 53, 38041 GRENOBLE cedex 09, France
[2]FaxénLaboratoriet, KTH, SE-10044 STOCKHOLM, Sweden

ABSTRACT

The aim of this paper is to assess the performance of a velocity measurement technique based on interferometry and using a cleaved mono-modal optical fiber. As this optical fiber is dived in a two-phase medium, interferometric signals are provided from the difference in optical paths between two light waves $\boldsymbol{E_1}$ and $\boldsymbol{E_2}$: a laser beam, injected inside the optical fiber from an external IR source, is separated into two waves because of the refraction at the end of the optical fiber; the first wave $\boldsymbol{E_1}$ is merely reflected at the end tip of the fiber whereas the second one $\boldsymbol{E_2}$ is transmitted and afterwards reflected by any incoming gas/liquid interface such as bubbles. The subsequent frequency-modulated signals (or Doppler bursts) lend themselves to a spectral processing allowing to assess the velocity of the bubbles. The hydrogen bubbles involved in this study are generated electrochemically so as to promote a mono-dispersed bubbly Poiseuille flow inside a straight vertical channel. Such an electrochemical generation allows to provide a typical diameter of the bubbles small enough to prevent them from any puncture by the optical fiber. These small bubbles, here referred to as micro-bubbles, behave as rigid spheres since 1.) the Weber number, the Bond number and the capillary number are all very small (of the order of 10^{-3} or less) and 2.) the surrounding salty liquid medium is contaminated by natural surfactants (coalescence of the bubbles is hindered). The optical signals suggest a passive behavior of the micro-bubbles with respect to the continuous phase streamlines around the optical fiber. If the bubble-Reynolds number increases up to Re~20, some of the micro-bubbles bounce upon the end tip of the optical fiber. In the case of bouncing, the subsequent signals exhibit two Doppler bursts: the first one is related to the incoming bubble interface whereas the second one is related to the backward motion of the bubble after bouncing. Whatever the shape of the optical signals (by-pass or bouncing signals), the numerical and analytical developments led by Dagan *et al* (1982) and O'Neill (1995) allow to develop a data processing relevant to our optical signals. In particular, it is possible to compute the bubble velocity far upstream the fibre.

* ruben@mech.kth.se
** laurent.davoust@hmg.inpg.fr

Introduction

As always in two-phase hydrodynamics, a systematically dogged information is the *ad hoc* closure law which allows to predict the drag exerted over one typical bubble "plunged" among others inside a bubble swarm (hindrance effect). The motion of a bubble with respect to the continuous phase is then shifted by a factor referred to as the slip velocity: a valuable data whose measurement has to be accurately performed. Subsequently, the first experimental step to overcome is the velocity measurement of the dispersed phase. This measurement, if performed by the way of conventional laser techniques (LDA, PDPA …), is by far more difficult within electrochemically-generated bubbly flows since they are typically characterized by a large interfacial area density (Γ~500-1000), a large concentration of the dispersed phase and a small size of the H_2-bubbles (diameter 2a~100μm). The use of a fiber-optics as a velocimeter allows to free oneself of typical issues such as light attenuation or scattering of the laser beams encountered with laser anemometers as soon as the optical paths are significantly long or the interfacial area density is large (Ohba *et al*., 1976).

The application of a cleaved optical fiber (core diameter~9μm, outer diameter~125 μm) to bubble velocity measurements is not widespread at present. Podkorytov *et al*. (1989) pointed out the ability of a cleaved fiber-optic to deliver Doppler bursts during the nucleation process of bubbles in cryogenic applications. Sekoguchi *et al*. (1984) are the only authors to our knowledge who tried to assess the velocity of some isolated gas inclusions by the way of cleaved multi-modal fiber-optics. The involved gas inclusions are, in both former studies, punctured by the cleaved fiber. Consequently, two small Doppler bursts superimpose to a typical two-levels signal when using protruded fiber-optics in two phase flows: the change in the refraction indices between gas and liquid is responsible for such a classical two-levels signal. Nevertheless, no detail about the spectral content of the signal is given in literature: only the more energetic frequency of the two Doppler bursts is seen by Sekoguchi *et al*. (1984) as a convenient way to assess the velocity of a bubble.

The experimental investigation presented in this paper is devoted to micro-bubbles. The electrochemical generation provides a typical diameter of the bubbles small enough to prevent them from a puncture by any standard optical fiber even if the typical size of the mono-modal fiber here-involved is small. Our hydrogen micro-bubbles behave as rigid spheres since the Weber number, the Bond number, and the Capillary number, are all small. To our knowledge, the optical signals so-obtained from the interaction between a micro-bubble and a cleaved mono-modal fiber-optics are new. Their particular shape seems to be in qualitative agreement with a quasi-passive behavior of the micro-bubbles with respect to the continuous phase flow streamlines around the fiber: the observed signals can be explained assuming that the bubbles bypass the fiber. Such a by-pass process is made evident through 1.) the absence of any two-level shape on the recorded signal and also 2.) the observation of one single Doppler burst for each bubble. Moreover, the frequency-modulation observed in the Doppler bursts is well-explained by the presence of a local stagnation flow at the end tip of the fiber located axially against the flow. Additionally, some experimental details are also given about what we call bouncing: such an encounter *scenario* holds as soon as the bubble Reynolds number reaches larger values (Re~20). In this case, the micro-bubbles bounce upon the tip of the fiber-optics and the subsequent signal exhibits two successive Doppler bursts.

The optical technique

A mono-modal optical fiber has been used for the detection of gas-liquid interfaces. Especially has the ability to measure the velocity for an interface which approaches the fiber tip, been investigated. In order to explain the optical technique, we assume a bubble of radius a, as displayed in figure 1., which is approaching the fiber tip whose radius is b. The bubble has a velocity V, parallel to the fiber, and the surrounding liquid has a velocity U_∞ which is, by definition, undisturbed by the presence of the fiber and the bubbles. The trajectory of the bubble points towards the centre of the fiber tip. An IR laser beam with wavelength λ_0 = 832 nm in vacuum, is guided into the core of the fiber. This beam is here referred to as $\boldsymbol{E}$. When the beam is partly reflected at the perpendicular end of the fiber, another part is transmitted through the end, reflected at the next interface on its way - the bubble surface- and, by assumption, returned back into the fiber.

The part of the beam, which is reflected immediately in the fiber end, is named $\boldsymbol{E_1}$ and can be described by the following expression

$$E_1 = A_1 e^{-i2\pi\nu t}, \qquad (1)$$

in which A_1, ν and t denote respectively the amplitude of the light wave, its frequency and time. The other part of the beam, referred to as $\boldsymbol{E_2}$, is transmitted through the end of the fiber, reflected on the incoming interface of the bubble, and then assumed to re-enter the fiber. Due to the extra optical path $?Sn_m$ travelled by the light, the expression for $\boldsymbol{E_2}$ involves a phase-shift $\Phi(t)=?Sn_m/c_0$:

$$E_2 = A_2 e^{-i2\pi\Phi(t)} e^{-i2\pi\nu t}. \qquad (2)$$

Here ?S=2(d-a) is twice the distance between the fiber tip and the bubble surface, n_m is the refraction index for the surrounding medium and c_0 is the celerity of light in vacuum. The sum ($\boldsymbol{E_1} + \boldsymbol{E_2}$) multiplied by its own conjugated expression $(\boldsymbol{E_1} + \boldsymbol{E_2})^*$ is the intensity ; as a matter of fact, the output voltage supplied by the photoreceptor is proportional to this

intensity,

$$\text{Voltage} = k\left[A_1^2 + A_2^2 + 2A_1A_2\,\text{Cos}\left\{4\pi(d-a)\frac{n_m}{\lambda_0}\right\}\right], \tag{3}$$

were k is a calibration constant. When an interface is moving towards the fiber, the spectral content of the interferences between $\boldsymbol{E_1}$ and $\boldsymbol{E_2}$ gives the motion history during the acquisition time. In other words, the voltage output is collected by an acquisition system (figure 3), and the instantaneous frequency of this signal,

$$f = \frac{1}{2\pi}\frac{d\Phi}{dt} \tag{4}$$

allows to assess the velocity of the incoming interface using

$$V_{op} = \frac{f\,\lambda_o}{2\,n_m}. \tag{5}$$

As shown hereafter, this spectral content can be used to determine the velocity of the bubble (Sekoguchi & Takeishi, 1984, Davoust *et al*, 2000).

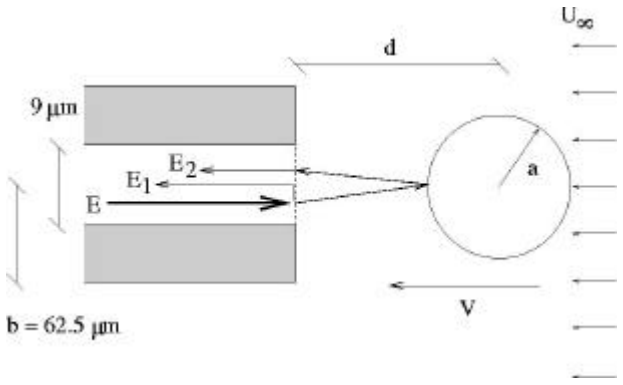

Figure 1. Motion of a bubble towards an optical fiber: the bubble interface reflects the light.

Interpretation and data processing of the optical signal

The approach of a micro-bubble

Several points are worth being mentioned. First, the intensity of the reflected beam is strongly dependent on the interface curvature. A large curvature, characteristic of a micro-bubble, will scatter the beam $\boldsymbol{E_2}$ in a wider solid angle than a plane interface. Secondly, the larger a bubble is, the larger the probability is to reflect the laser beam. In other words, the size of the bubble is an important parameter. Finally, the way the interface approaches has a huge influence on the quality of the optical signal : the alignment of the bubble with the optical fiber stands as a relevant parameter (figure 2.).

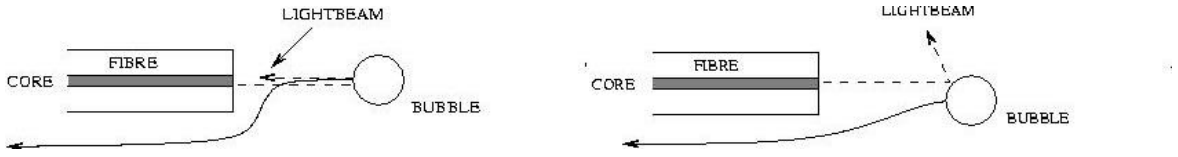

Figure 2. (Left) The trajectory of a bubble, transported against the core of the fiber with a good alignment. The bubble approaches closely to the fiber end and the light beam is reflected towards the core.
(Right) The trajectory of a bubble, transported against the core of the fiber with a poor alignment. The bubble starts turning for the fiber end on a large distance and the light beam is mostly reflected away from the core.

An optical signal delivered by a micro-bubble is given in figure 3a. The useful part of the signal is distinguished from noise by the possibility to identify a frequency physically relevant in the spectral content (see *e.g.* figure 3b). The increase in the amplitude of the signal is a measure of the intensity of the reflected beam $\boldsymbol{E_2}$; the intensity level depends mainly on the

distance between the approaching interface and the fiber tip. An amplitude fall can be observed on the signal just after the maximum in intensity. The explanation we put forward is the quick change in the reflection angle of $\boldsymbol{E_2}$ when the bubble shifts its lateral position by-passing the fiber. This last stage of the bubble dynamics has not been studied neither from the viewpoint of hydrodynamics nor from the viewpoint of optics and signal processing. Most of our efforts have been done to produce a spectral analysis of the signal when the straight trajectory of the bubble reaches the fiber ; this stage is connected to the primary part of the optical signal, before the maximum in intensity. The first logical step is now to analyse the frequency of the oscillations in the signal and to present the frequency as a function of the time. An usual FFT, (Fast Fourier Transform), cannot be applied since the information of time has to be kept. However, by using FFT sliding window, the desirable goal is reached. The figure 3b shows the frequency f, equation 4, as a function of time. For the further approximate analysis, we also wish to get rid of singular frequency points that do not follow the main frequency trend: it is convenient to remove the non-physically relevant frequencies due to noise. The only effect of this de-noising process is that the analyse procedure is easier to automate. The accuracy of the result is not expected to be affected. The second logical step is then to calculate the velocity, equation 5, from the instantaneous frequency. Finally, the calculated velocity V_{op} is scaled with a reference velocity V_{ref} , here chosen to be the measured averaged liquid velocity in the test channel. The subsequent non-dimensional velocity is plotted on figure 3c. It can be seen that the asymptotic velocity is not reached. Apparently, the light intensity is too weak to reach the bubble when it was moving far upstream the fiber. In other words, the depth of detection of the optical sensor is too small to catch the undisturbed optical velocity $V_{op\infty}$.

The approach of slugs and flat interfaces

A flat interface has an infinite radius of curvature, and the whole of the beam $\boldsymbol{E_2}$ is assumed to re-enter the fiber after its reflection on the rising interface. A slug has a large, but not infinite, radius of curvature. Since the proximity of the fiber does not change the velocity of the incoming flat interface or slug, both optical signals resemble each other. If the velocity of the approaching interface is externally imposed to be constant, it is possible to estimate the depth of detection for the fiber. As usual with the optical fibers devoted to the gas hold-up measurements, after the puncture of the interface of a slug or a flat interface by the fiber, the mean level of the optical intensity changes. This is due to the difference in refraction index between the two involved mediums (salty water, air). An optical signal for a slug is given in figure 4.

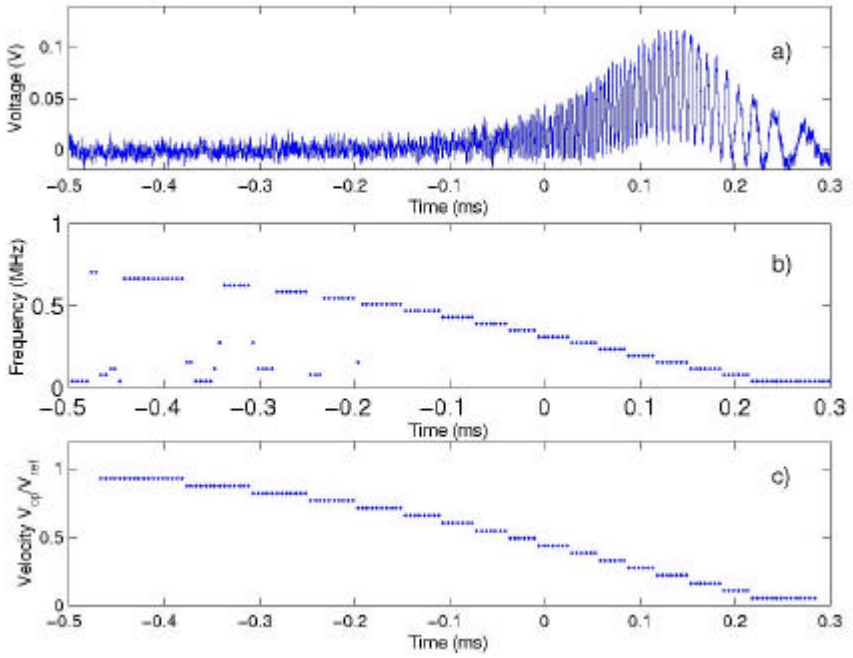

Figure 3. Processing of an optical signal delivered by micro-bubble.
(a) The signal of an approaching bubble, acquired by the acquisition system. (b) FFT/sliding window analysis of the signal. (c) Noise is removed from the spectral content, the subsequent frequency is transformed to the velocity V_{op} *and scaled with a reference velocity* V_{ref}.

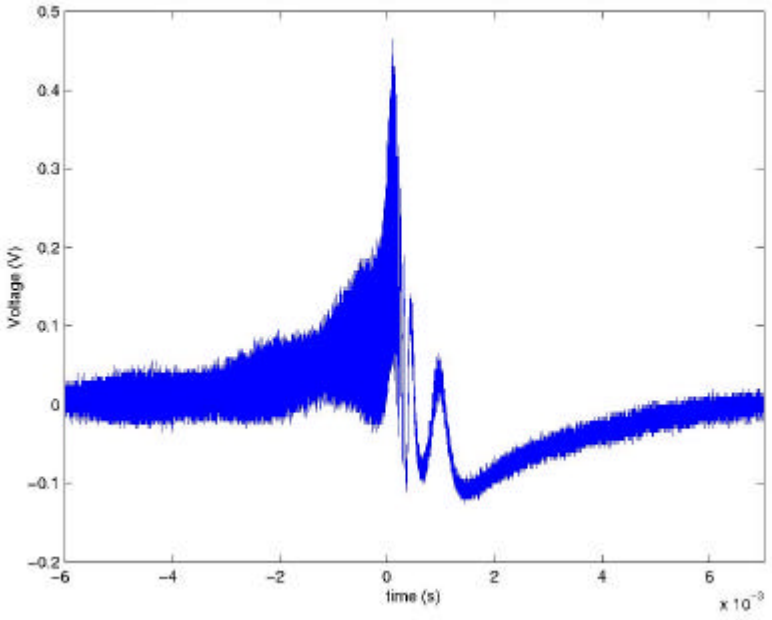

Figure 4.The signal of a slug approaching with velocity V_{ref} *=6 cm/s.*

The Experimental Set-up

The experimental set-up, figure 5, consists of a vertical test channel of rectangular cross-section (8.5mm x 10mm), and an downwards/upstream pointing optical mono-modal fiber (outer diam. 125µm and core diam. 9µm) located at the top of the channel. The voltage output supplied by the HAMAMATSU photodetector is filtered and connected to the data acquisition system INSIGHT.

A set-up was used in which the gravity transports the electrolyte from a high positioned tank to the low positioned exit of the test channel. The velocity was controlled by 1) the difference in height between the tank and the test channel and 2) a valve on the connecting tube. After the passage of the optical fiber, the volumetric flowrate was measured with a graded glass and a chronograph.

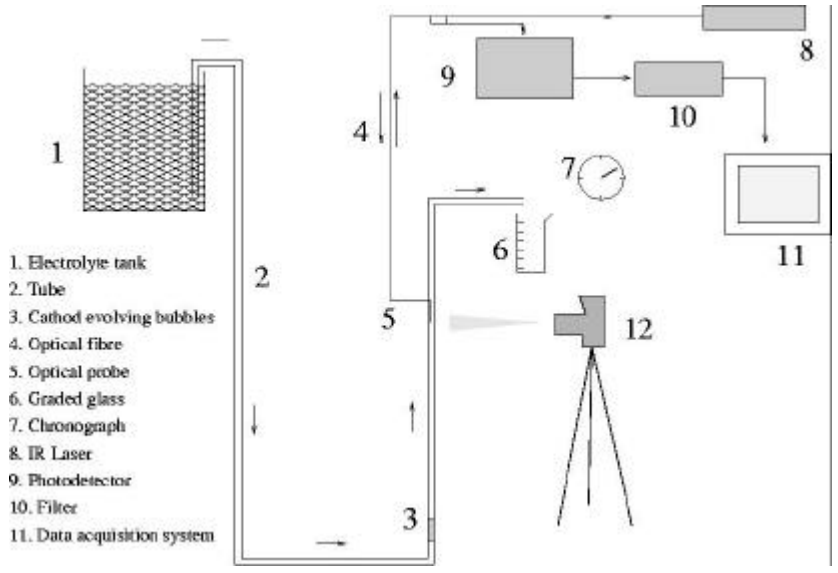

Figure 5: The experimental set-up.

The micro bubbles are electrochemically generated with a cathode close to the bottom of the test channel. This position provides a sufficiently short transport distance from the production site to the fiber end to prevent bubble coalescence. A small opening in the wall just below the electrodes allows the necessary free passage of electrically charged ions between the cathode and the anode, while at the same time preventing from any leakage of oxygen bubbles generated at the anode. As an electrolyte, we have used a low concentration of sodium sulphate in water. The refraction index, the density and the viscosity are very close to the physical characteristics of water.

Measurements of the velocity V_{ref}

Plane front approaching the fiber. The liquid interface was released upwards towards the tip of fiber, and the reference velocities were achieved by: (a) Image analysis of the filmed sequence, (b) manually measuring the time when the front travels a known distance.

Long slugs passing the fiber. The liquid velocity was controlled by an air/water pressure tank with adjustable valves connected to a vertical test tube of circular cross-section. The reference velocities were obtained by a laser and two photodetectors connected to a digital time meter.

Electrochemically-generated bubbles. The buoyant micro-bubbles were transported by liquid flow forced through the test channel. The reference velocities were deduced from the volumetric liquid flow. The small bubbles were produced in the channel. In connection to the reception of an optical signal, the volumetric liquid flow was measured with a graded glass and a chronograph.

Experimental results

Measurements of the velocity for plane fronts and slugs

Due to the flatness of the plane fronts and their constant approach velocity, we expect a good response of the optical sensor. Signals from plane fronts were investigated covering the range $10 < Re_H < 1160$. The Reynolds number is defined as $Re_H = V_{ref} D\rho_l / \mu_l$ where $0.3 < V_{ref} < 12.6$cm/s is the range of the rising velocity for the plane fronts along the channel, D (= 4Area/circumference =9.2mm) is the hydraulic diameter, $\rho_l = 10^3$ kg/m^3 and $\mu_l = 10^{-3}$ kg/ms are respectively the density and the viscosity of the liquid. In addition, we collected signals from slugs in the range $526 < Re_H < 4800$, *i.e.* $5.7 < V_{ref} < 52.3$cm/s. As aforementioned, both the plane fronts and the slugs approaches the fiber end in a straightforward motion and with an efficient reflection of the laser beam. Each signal has been analysed by the technique of sliding window FFT to achieve a velocity V_{op}. The figure 6 displays a comparison between the velocities V_{op} and the reference velocities V_{ref}. Considering the error in the three different sets of experimental data, the agreement is acceptable.

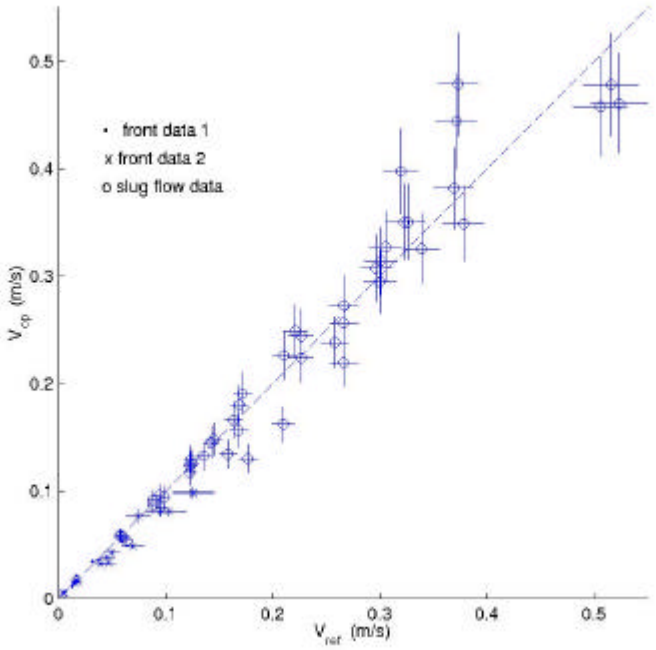

Figure 6: The velocities V_{op} , detected with the optical fiber, versus the reference velocities V_{ref}
Front data 1: Plane gas to liquid interface V_{ref} *, measured with the technique of image analysis.*
Front data 2: Plane gas to liquid interface V_{ref}*, measured manually with chronograph.*
Slug flow data: The front of an air slug in water V_{ref} *, measured with a transit time technique.*

The depth of detection

We can, from the experiments with plane fronts and slugs, also estimate the maximum depth of detection by the optical fiber. By integrating the received velocity V_{op} over time, we can get an assessment of the distance. As a criterion for the relevant time of the signal we have a demand on the amplitude to continuously be 30% over the amplitude of the noise. A second demand is that the frequency is clear enough to be analysed during the actual time period. As seen in the figure 4, the amplitude seems to be somewhat pulsating. Some signals has been sampled where pulses of increased amplitude and visible frequency were found a long time before the "real" interface signal begins. It is our believe that these pulses are due to either small reflecting micro particles in the fluid or flashes of reflections from the slightly vibrating interface far away. The depth of detection was found to be around 0.3 mm., a depth that appeared to be independent of the velocity of the interface. The same results were achieved both for plane fronts and for slugs. This depth of detection was later verified in complementary experiments when the fiber was stepwise descended towards and through a water surface at rest, figure 7.

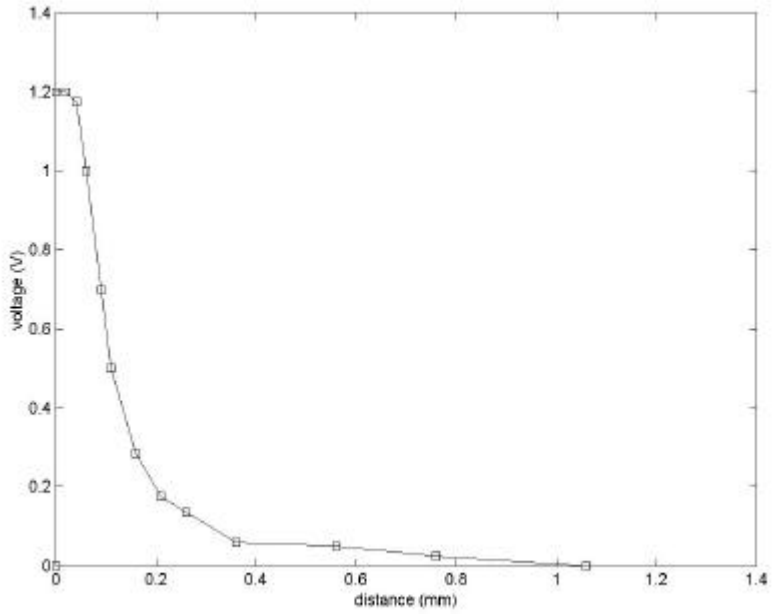

Figure 7: The intensity of the signal for different distances to the air/water surface; the probe is in air.

Measurements on micro bubbles

After these first results, a few experiments have been done with micro-bubbles. As previously described, the curvature of the bubble surface will most likely cause optical signals with much less intensity. A short radius of curvature, which scatters the laser beam, and a bubble trajectory, which is largely affected by the vicinity of the fiber, stand as two factors that make the signal analysis more difficult than for a flat front.

With the purpose to get first an estimation of the size of the micro bubbles, the test-channel was filmed during operation. By using image analysis with several flow rates of the electrolyte, the typical bubble sizes can be estimated. It has been found that the bubbles size is only slightly dependent on the flow rates of the electrolyte. As revealed by the histogram displayed on figure 8, the diameter of the bubbles was found to be about 110±40 µm. As a matter of fact, our observations showed that the carried bubbles moved in straight paths within the channel with negligible lateral fluctuations.

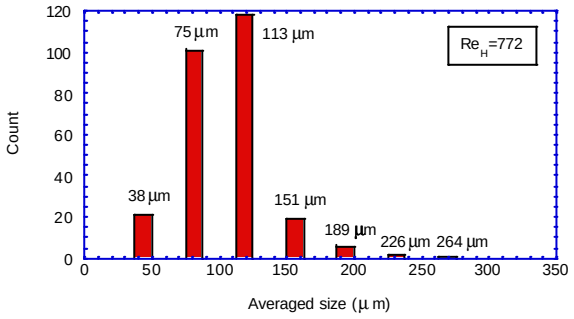

Figure 8: Histograms of typical bubble sizes received by image analysis..

We have also performed optical measurements in the range $600 < Re_H < 2900$ *i.e.* an averaged velocity V_{ref} = 6.9-31 cm/s. From the analysis of these optical signals it is found that none of the signals allows to directly measure the asymptotic bubble velocity far upstream from the fiber. It is clear that further analytical developments should help to extend the received optical signal up to the expected velocity.

A first analytical tool to predict the approach of a bubble

In order to predict the velocity of the bubble a few bubble radius upstream, we used the theory by Dagan *et al.* (1982). These authors combined analytics and numerical calculations in order to compute the creeping motion of a spherical particle in the stagnation flow generated by a flat disk. While their work was focused on a neutrally buoyant sphere carried by the fluid towards the disk, we have considered a micro-bubble. Consequently, the buoyancy force for the bubble was added to the theory by Dagan *et al*. Other forces could be invoked as important for the motion *e.g.* the added mass force. For simplicity, we have, however, neglected the introduction of such other forces. We have also assumed that the results are valid when the disk, as in our case, has a thickness much larger than the radius. Following the notation defined in figure 1., the creeping motion of the bubble obeys

$$\Lambda + 6\pi a' \left[V' \lambda^{(V')}_{(a',d')} + U'_{\infty} \lambda^{(U'_{\infty})}_{(a',d')} \right] = 0 \,, \qquad (6)$$

where $?^{(V')}_{(a',d')}$ and $?^{(U'_{\infty})}_{(a',d')}$ refer to as the instantaneous hydrodynamic interaction coefficients tabulated by Dagan *et al*. These coefficients depends on the non-dimensional bubble radius a'=a/b (b is the disk radius, figure 1), and on the instantaneous distance d'=d/b between the bubble and the disk. Moreover, $?=4\pi a^3 g\rho_l^2/3\mu_l^2$ stands as a non-dimensional group measuring the balance between the buoyancy force and the viscous force. The quantities $V'=V\, b\rho_l/\mu_l$ and $U'_{\infty}=U_{\infty}\, b\rho_l/\mu_l$ are the non-dimensional velocity of the bubble and the non-dimensional velocity of the fluid at infinity. With the knowledge of the bubble radius a, the former equation can now be solved for the unknown velocity V. To illustrate the typical behaviour of the velocity V close to the fiber, a few curves are displayed on the figure 9.

The idea is to investigate whether it is possible to fit the optical signal with the theoretical prediction for the bubble approach and thereby to find the undisturbed velocity V_{∞} of the bubble. With the knowledge of either the bubble radius a or the velocity U_{∞} of the liquid at infinity, the fitting process is straightforward and can quickly be achieved through a trial and error procedure. In the experiments, however, are both the bubble size and velocity unknown. Therefore we must try to fit both parameters at the same time. As a matter of fact, since both the bubble radius and the velocity at infinity stand as sensitive parameters to the adaptation process, one combination of them causes a unique bubble motion history. If we succeed to find the unique values for a and U_{∞} that fit the theoretical bubble velocity history to the measured one we can obtain the bubble velocity. Since, however, the coefficients $?^{(V')}_{(a',d')}$ and $?^{(U'_{\infty})}_{(a',d')}$ only cover the region up to d/a=10, where the acceleration most often has started, we must assess the undisturbed bubble velocity as $V_{\infty}= U_{\infty}+V_{relative}$, *i.e.* by adding the terminal rise velocity $V_{relative}=2a^2\rho g/9\mu$ to the achieved liquid velocity in infinity U_{∞}.

As an illustration, six fitted curves are displayed on figure 9. The non-dimensional velocity and time exhibited on this figure are obtained from the following scales: the ratio $(\mu_l/ b\rho_l)$ for the velocity and the ratio $(b^2\rho_l/\mu_l)$ for time.

As given in the table 1, the velocity U_{∞} was found to be 20-30 % higher than the averaged velocity V_{ref} measured simultaneous in the experiments. The bubble radius a was found to be approximately 130 µm. This value is high compared to the data presented in the former figure 8. Two explanations can be put forward : either the larger bubbles give rise to an optical signal more frequently, or the analytical model we have used has to be refined further. Considering now the simplifications involved in this first investigation, the results are, however, satisfactory, and the proposed method is a promising tool for the measurements of size and velocity of micro-bubbles in situations where conventional LDA technique can not be applied (high interfacial area density).

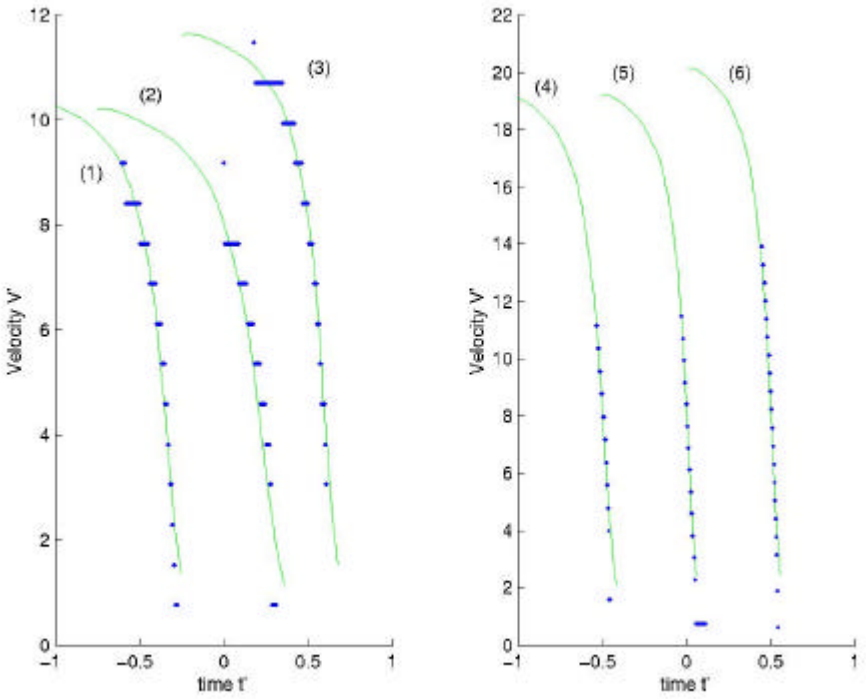

DAGANANALYSE.JPG

Figure 9: Adaptation of optical signals for micro bubbles with analytical prediction. Non-dimensional time and velocity for optical signal (dots) and equation 6 (solid line).
(left) The curves (1)-(3) displays three signals with Re_H *= 925, 970 and 1120.*
(right) The curves (4)-(6) displays three signals with Re_H *= 2160, 2300 and 2350.*

Curve no.	V_{ref} (cm/s)	U_∞ (cm/s)	radius a (μm)	V_∞ (cm/s)
1	10,6	13,5	140	17.8
2	10,1	14,5	120	17.6
3	12,1	15,5	140	19.8
4	25.0	30.0	120	33.1
5	23,5	29.0	135	33.0
6	25,6	31.0	130	34.2

Table 1: Corresponding values to the figure 9. The measured reference liquid velocity V_{ref} *, together with the adapted values for velocity* U_∞*, bubble radius* a *and undisturbed velocity for the bubble, all three deduced from fitting with the theoretical prediction.*

The bouncing bubble

As the typical Weber number of the micro-bubbles is very small (less than 10^{-3}), an other kind of optical signals has been made evident as soon as the bubble Reynolds number increases up to 20. Such new optical signals (see figure 10) are attributed to the bouncing of the micro-bubbles at the tip of the fiber. Consistently, bouncing of bubbles has also been identified with ordinary bubbles (size of the order of 1 mm) by Tsao & Koch (1994, 1997) as soon as the bubble Reynolds number is significantly high. An FFT sliding window has been applied to one of our bouncing optical signals. If one focuses on the signal at the time when the interface velocity vanishes (time $t=2\cdot10^{-3}$ s in the figure 10), it is easy to note how the velocity is symmetrical around this time. The mere explanation which comes to mind is the conservation of the mechanical energy. The sum of the kinetic energy (driven by the liquid added-mass behind the bubble) and the potential energy (due to the weak interfacial deformation of the bubble) is then conserved at the impact of the micro-bubble with the fiber. That suggests that viscous dissipation arising during the draining of the interstitial liquid film located between the bubble and the fiber is negligible. And finally, since our bubbles are very small, deformation of the interface is so small that the measured velocity of the micro-bubble interface can be seen as approximately same as the actual micro-bubble velocity.

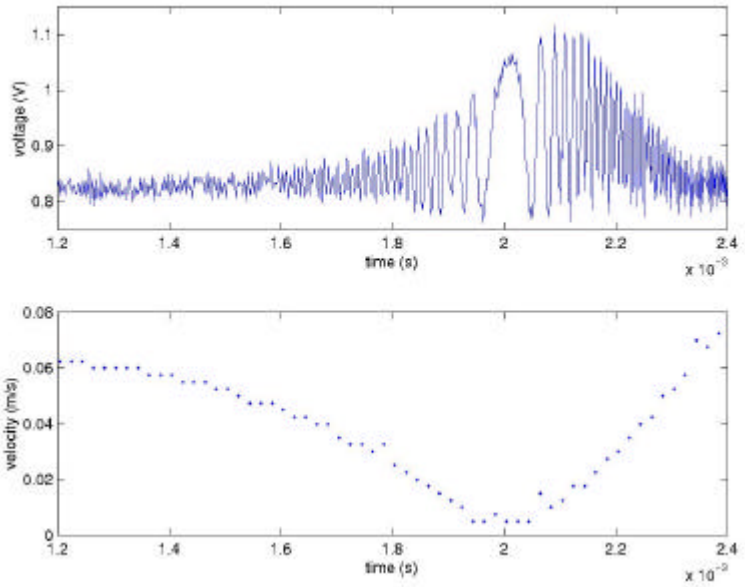

Figure 10: Bouncing of a bubble at the optical fiber end. (a) The optical signal acquired by the acquisition system. (b) The velocity of the micro-bubble interface calculated from the signal.

Conclusions

We have investigated the ability of a mono-modal optical fiber to measure the velocity of moving gas-liquid interfaces such as slugs or micro-bubbles. Such a measurement technique offers *a priori* the potential to be used inside high concentrated two-phase mixtures whereas any ordinary LDA measurement is otherwise difficult to perform (high interfacial area density, diffusion of the laser beams). Using a cleaved optical fiber, the light is reflected both at the tip of the optical fiber and at the incoming gas-liquid interface outside the fiber. This latter part, while it re-enters the fiber, interferes with the former part. A time-frequency processing of the optical signals allows to assess the velocity of the moving gas-liquid interface versus time. Experiments have been performed with flat fronts, slugs and micro-bubbles flowing vertically towards a downwards-pointing optical fiber.

For flat fronts and slugs in constant motion, it was found that the velocity of the approaching interfaces can be measured with an acceptable precision. The depth of penetration has been estimated and found to be roughly 0.3 mm, a sensitivity length that seems to be at first sight independent on the velocity of the incoming interface. Continuous experiments were also carried out with micro-bubbles. These bubbles were produced by an electrochemical reduction of a dilute sodium sulphate solution. From an image analysis, the typical bubble diameter was found to be 110± 40µm and did not vary significantly with the velocity. The intensity of the optical signal was found to be much lower than for the experiments involving both slugs and plane fronts. This is partly explained by the large divergence of the reflected light at the bubble surface due to its small radius of curvature. Since the typical detection depths for the bubbles is too low to catch the undisturbed velocity of the bubble far upstream of the optical fiber, a method of extrapolation based on analytical

developments is presented. This method is inspired from an analytical/numerical work performed by Dagan et al. 1982, devoted to the creeping approach of a spherical particle at the vicinity of a flat disk. Mixing these theoretical ingredients with a time-frequency analysis of our optical signals, it is possible to infer both the bubble size and the undisturbed velocity. To improve the accuracy, a more realistic bubble dynamics has to be considered, by introducing notably the added mass.

References

Dagan Z., Pfeffer R. and Weinbaum S., 1982, *Axisymmetric stagnation flow of a spherical particle near a finite planar surface at zero Reynolds number*, J. of Fluid Mech., **122**, pp. 273-294.

Davoust L., Achard J-L. and Cartellier A., 2000, *Detection of waves at an interface by the way of an optical fibre*, to appear in Prog. Colloid Polym Sci.

Ohba, K., Kishimoto, I. and Ogasawara, M., 1976, *Simultaneous measurement of local liquid velocity and void fraction in bubbly flows using a gas laser*, Tech. Rep. Osaka Univ., **26**, pp. 547-556

O'Neill, M.E., 1996, *On the modeling of particle-body interactions in Stokes flows involving a sphere and circular disk or a torus and circular cylinder using point singularities*, Chem. Eng. Comm., **148-150**, pp. 161-182

Podkorytov, D.G., Timkin, L.S. and Chinnov, Y.A., 1989, *A fiber-optics method for investigating boiling in cryogenic fluids*, Soviet Journal of Applied Physics, **3**, pp. 136-144

Sekoguchi, K., Takeishi, M., Kano, H., Hironaga, K. and Nishiura, T., 1984, *Measurements of velocity and void fraction in gas-liquid flow with an optical fiber*, paper 16-1, 2nd International Conference on laser Doppler Anemometry, 2-4 July, Lisbon.

Tsao H-K. and Koch D.L., 1994, *Collisions of slightly deformable high Reynolds number bubbles with short-range repulsive forces*, Phys. Fluids, **6** (8), pp. 2591-2605

Tsao H-K. and Koch D.L., 1997, *Observations of high Reynolds number bubbles interacting with a rigid wall*, Phys. Fluids, **9** (1), pp. 44-56